Pyrogenic HONO seen from space: insights from global IASI observations.

https://doi.org/10.5194/egusphere-2023-2707

Response to Referee #1

The paper by Franco et al. presents pyrogenic nitrous acid (HONO) detection and total column quantification based on satellite observations from IASI on Metop since 2007. The detection method is based on the hyperspectral range index to identify spectra with observable HONO signature. Two spectral regions are investigated (820-890 cm-1 and 1210-1305 cm-1) to detect HONO in fire plumes and it is shown the 1210-1305 cm-1 band is the most sensitive because less affected by interfering species. An additional filter combining the HONO detection with ammonia (NH3) and ethylene (C2H4) detection, also emitted by fires, is proposed to limit false detections of pyrogenic HONO in IASI spectra. The paper provides an analysis of the pyrogenic HONO detections in terms of spatial and temporal distributions from the entire archive of IASI A, B, and C instruments and compares the results with the TROPOMI HONO product available at the end of the period and to MODIS fire products. The IASI HONO detection is the most reliable for the mid and high latitudes of both hemispheres. The reasons of the low detection rate in the tropics are discussed. The paper highlights the increase of pyrogenic HONO detection during the last five years in agreement with the increase of wildfire activities. Finally, the paper proposes an estimation of HONO total columns using an artificial neural network architecture, already applied to other low-absorbing species retrieved from IASI. A tentative of comparison with TROPOMI HONO columns estimation is provided for two case studies, and the limitations of such comparisons are discussed.

The paper provides an important step forward in satellite remote sensing of wildfire impacts on atmospheric composition, focusing on a challenging species, HONO. Nitrous acid is a key atmospheric species as a major source of hydroxyl radical, but important gaps remain in our knowledge of its global budget due to the difficulties to measure it at large scales. The new HONO IASI product presented in the paper complements the recent TROPOMI HONO product, especially with nighttime observations to probe globally HONO in pyrogenic plumes, and the long time series available is of great value to improve knowledge on HONO atmospheric budget. The paper is well structured, written and documented. The results are well argued, and limitations of the HONO product mostly discussed. The paper is suitable for publication in ACP after some clarifications.

We would like to thank the Referee for the positive evaluation of this paper and for the comments that contributed to improving the manuscript. Please find in blue here below our response to the comments and the changes made to the manuscript. Furthermore, we have revised several figures to improve both their clarity and consistency across the entire manuscript.

Main comments:

My main comments concern the description of the detection and retrieval approaches, which needs some clarifications. These approaches have been already described in other papers for other species and the authors referred to these papers, but some details are missing to understand the specificities to HONO detection and retrieval.

Concerning the detection method (section 2.1), it is not clear which assumptions are made on the atmospheric concentrations of HONO and interfering species to calculate the Jacobian K. We understand later in the text (line 376) that the US 1976 standard atmosphere is used as well as a HONO profile including a narrow layer (line 375) but without much more details. Is the HONO profile considered as a gaussian profile, as described in section 4? What is the impact of the shape and the height of the HONO peak on the detection based on the HRI? These details should be provided earlier in the text (section 2.1) and completed. The authors should also specify how they calculate the generalized covariance matrix Sy. Is this matrix diagonal, for example?

The HONO detection with the HRI is not significantly influenced by the assumed profile and abundance of HONO or the atmospheric conditions that were used to construct the Jacobian. This is illustrated in the figure below, which displays, in blue, the Jacobian used in this study, which has been generated based on a HONO total column of 1.77 x 10^{17} molec cm^{-2} confined to a narrow layer (~1 km thick) at 2 km altitude, assuming the US 1976 standard atmosphere. The second Jacobian, in red, has been generated assuming a HONO total column more than one order of magnitude lower (7.03 x 10^{15} molec cm^{-2}), confined in a half-thickness layer at 4 km altitude, for a mid-latitude atmosphere in summertime. The figure below shows that all these changes do not significantly affect the intensity of the Jacobian, nor does it change its shape.

Please note that Lines 375-376 do not refer to the Jacobian that is used to calculate the HRI, but instead to different Jacobians that are generated specifically for calculating the IASI's detection threshold of HONO for various altitudes through Eq. 6. In this specific case, a Gaussian profile was assumed, peaking at various altitudes between 0 and 14 km, and with a standard deviation (σ) of 300 m representing a narrow atmospheric layer.

We have detailed the calculation of the covariance matrix as follows:

"*This set of background spectra, and the associated S_y and $\bar{y}$, are determined via an iterative filtering process (Franco et al., 2018; Clarisse et al., 2019). Beginning with a comprehensive set of IASI spectra, this process consists, at each step, in calculating S_y and $\bar{y}$ associated with the given spectra, determining the HRI for each observation, discarding all spectra with detectable target gas signatures from the set, and calculating the factor N.*"

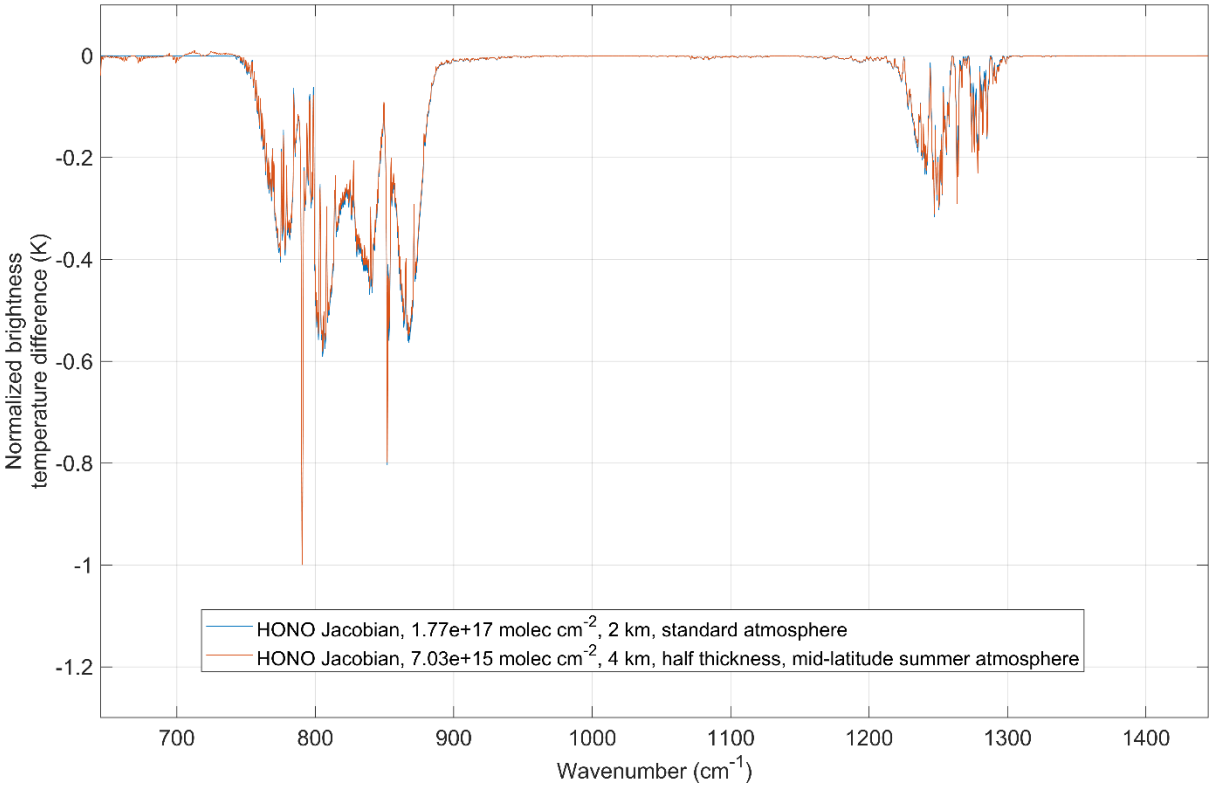

Similarly, the set-up for the retrieval of HONO in section 4.1 is confused. It is not clear for me what are the inputs and the outputs of the NN. Indeed, it is not described how the parameters related to the abundance and vertical distribution are chosen to feed the NN and if they are retrieved at the output of the NN or if it is just the total columns. Line 517 it seems these parameters are variable from one pixel to another in the inputs (on which basis/assumption these variations are chosen? Is a model used?) but line 523, it seems that σ is fixed to 350m for all the pixels without any discussion of this choice, whereas a range of possible variations from 100m to 3km is mentioned in Eq 8. This should be clarified.

We now better explain in Sect 4.1 what the inputs and outputs of the NN for the HONO retrieval are, and we clarify how the parameters z_0 and σ are defined:

"The first step of the ANNI retrieval procedure consists in calculating an HRI for each observed spectrum, as described earlier (Sect. 2.1). In the second step, each HRI is converted into a single pixel estimate $\hat{X}^a$ of the gas total column via a scaling factor SF^a (the superscript a indicates the use of an assumed vertical distribution of the target gas):

$$\hat{X}^a = {HRI}/{SF^a} \qquad (7)$$

In ANNI, SF^a is estimated by an artificial feedforward neural network (NN) that considers the state of the Earth's atmosphere and surface. For a given IASI observation, the NN input parameters include the HONO HRI itself, the temperature (15 levels) and the H_2O (7 levels) profiles, surface temperature, pressure, emissivity, and the IASI viewing angle associated this observation. In addition, two parameters z_0 and σ are provided to the NN to characterize the HONO vertical profile following a Gaussian distribution:

$$vmr_{HONO} = k \times exp\left(\frac{-(z-z_0)^2}{2\sigma^2}\right) \qquad (8)$$

with k a multiplicative factor, z_0 ranging from the surface up to 20 km altitude, and σ comprised between 100 m and 3 km. This vertical profile parametrization, which is the same as used for the NH_3 and C_2H_4 IASI products, allows to approximate a wide variety of profiles (Whitburn et al., 2016; Van Damme et al., 2021; Franco et al., 2022). In particular, for HONO, this profile can be used to model fire plumes of various thicknesses and located at various altitudes from the surface to the lower stratosphere.

The NN consists of two computational layers of 12 nodes. It is trained based on an extensive set of synthetic spectra (>500,000 spectra) generated with representative input data of the atmospheric and surface conditions as well as parameters related to the abundance and vertical distribution of HONO (σ, z_0, and k). For each IASI observation, the NN estimates SF^a based on the input parameters and provides the $HRI/\hat{X}^a$ ratio as the main output (along with other ancillary outputs; see Sect. 4.2), which is subsequently converted to $\hat{X}^a$. The primary advantage of using this ratio as output instead of $\hat{X}^a$ itself is to ensure that the retrieval on noisy HRI does not result in a biased product (see Whitburn et al., 2016, for more on the rationale behind this ratio).

For the ANNI retrieval, the meteorological input variables are sourced from the European Center for Medium-Range Weather Forecasts (ECMWF) ERA5 reanalysis (Hersbach et al., 2020). This choice ensures a more comprehensive and coherent dataset across the entire IASI operational time series than with the IASI Level 2 data (Van Damme et al., 2021).

Ideally, z_0 and σ should be tailored for each singe-pixel HONO retrieval based on the actual altitude and thickness of the fire plume. Unfortunately, such third-party information is rarely available. Consequently, for the standard ANNI v4 HONO product, the parameter z_0 is set based on a 1° × 1° monthly climatology of fire plume altitudes derived from CALIPSO data (Sect. 3.2), and a value of 350 m is assigned for σ. The same approach was applied to estimate the dust altitude for retrieving dust optical depths from IASI observations (Clarisse et al., 2019). However, since the NN has been trained to encompass a broad range of z_0 and σ values, these parameters can be adjusted for an optimized HONO retrieval if information on the altitude and thickness of a specific fire plume under study becomes available."

Specific comments:

Line 113: the authors could specify that the spectra in brightness temperature are considered for the HRI calculation.

The spectra are considered in radiance for the HRI calculation. However, in the manuscript, such as in Fig. 2, the IASI spectra shown as examples are displayed in brightness temperature as this unit is more convenient for display purposes.

Lines 170-171: trace gases and surface emissivity are mentioned but what about aerosol spectral signatures? Do they interfere with HONO signature?

In Clarisse et al. (2010, 2013), it has been shown that smoke aerosols in the thermal infrared are typically characterized by weak and broad spectral signatures spanning several hundred cm^{-1}, thus primarily affecting the spectral baseline. The effect of such aerosols on the IASI spectra is marginal because of the size of these particles. As a result, even for huge fires, IASI retrievals remain mostly insensitive to smoke aerosols. For instance, it can be seen in Fig. 2a and Fig. A3a (for fires in Canada and Portugal, respectively) that the baseline of the IASI spectra is not affected. So far, smoke aerosols have only been clearly identified in IASI spectra during the exceptional Australian fires. This is

illustrated in the new Fig. A2a (see our response to the next comment) by the noticeable change in the baseline of the IASI spectrum compared to the examples in Fig. 2a and Fig. A3a.

Lines 210-213: as up to now, detection of HONO with IASI was done only in Australian fires, it would have been interesting to provide an example of the magnitude of the HONO spectral contributions also in an Australian fire case to see how higher it is compared to other fires.

The figure below reproduces Figs 2 and A2, showcasing an IASI/Metop-A spectrum captured in a fresh fire plume during the 2019/2020 Australian wildfires. The spectral analysis aligns with previous conclusions drawn for other fire plumes presented in the manuscript, but the HONO HRI values here are notably elevated, reaching 36.04 and 56.62 in the first and second absorption bands, respectively. This underscores the exceptional intensity of this fire event. We have added this new figure to the Appendix and referred to it in Section 2.3 as follows:

"*For comparison, the spectral analysis of an IASI observation in a fresh Australian fire plume from December 2019 (depicted in Fig. A2) indicates markedly higher HONO HRI enhancements, with values of 36.04 for the 820-890 cm^{-1} range and 56.62 for the 1210-1305 cm^{-1} window.*"

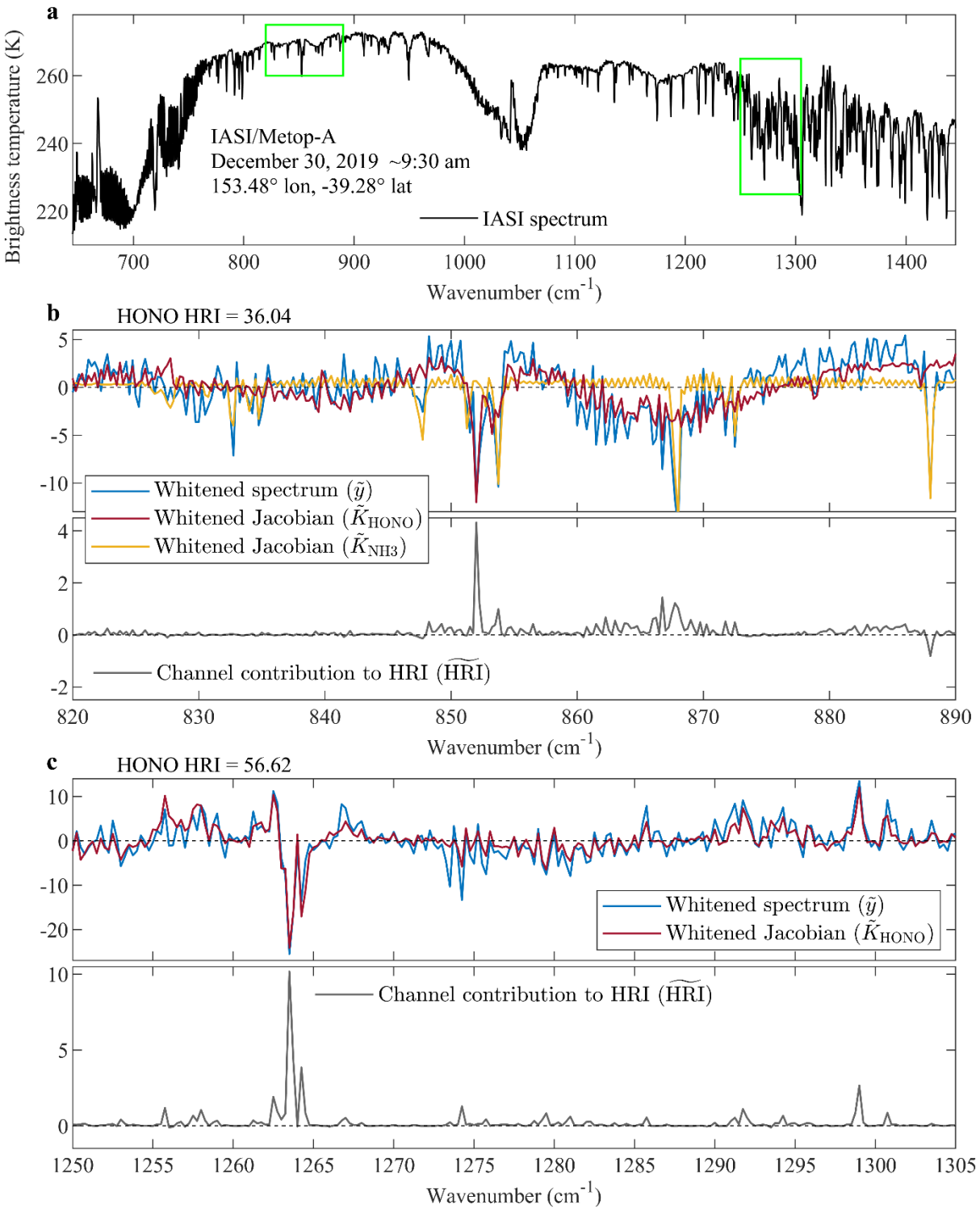

Section 2.4: The authors have demonstrated that the 820-890 cm-1 region is less sensitive to HONO detection compared to the 1210-1305 cm-1 region. What is the interest to provide the filter for this spectral region, which is not leveraged after? What would be the interest to use both regions for detection and retrievals?

We thank the Referee for this comment. Throughout Sect. 2, we conducted various exercises to evaluate both spectral ranges, including a comparison of HRI intensity in fresh fire plumes (Sect. 2.2),

a thorough spectral analysis with the whitening (Sect. 2.3), and a comparison of the specific detection filters set up for each absorption band (Sect. 2.4). While we concluded Sect. 2.4 by specifying our focus on the 1210-1305 cm^{-1} HRI for the rest of the study, we deliberately included some results from the 820-890 cm^{-1} range in our analysis in Sect. 3 (and related figures in appendix) as it allows us to perform comparisons between the two HONO bands. The consistency observed in our results across these two ranges provides indeed valuable cross-verification, bolstering the robustness of our findings. We are convinced that this approach is important for establishing the reliability of our methodology and results, and that it enhances the overall strength and credibility of our study. Please note, however, that the 820-890 cm^{-1} band is not used for the retrievals in Sect. 4.

To clarify our approach, we have added the following statements, respectively, in Sect. 2.1 and at the end of Sect. 2.4:

Line 132: "*Throughout Sect. 2, we systematically assess the advantages and limitations of each spectral range for the detection of pyrogenic HONO.*"

Line 278: "*Considering the advantages presented in Sect. 2 by the 1210-1305 cm^{-1} band for the detection of pyrogenic HONO with IASI, we will focus on the HRI calculated within this range from Sect. 3 onwards. Nonetheless, results obtained with the 820-890 cm^{-1} band will also be briefly presented, as they allow for important cross-verification.*"

Figure 5: IASI and TROPOMI are not compared for the same period (IASI since 2007, TROPOMI since 2018). Are the results different if the same period is used for the comparison?

Please find below a revised version of Fig. 5, using only the IASI data since 2018. It exhibits only marginal differences from the original Fig. 5, based on the entire IASI time series, and does not alter any conclusions of the analysis. For consistency, only the MODIS data since 2018 are displayed. We are now using this revised version of Fig. 5 in the manuscript.

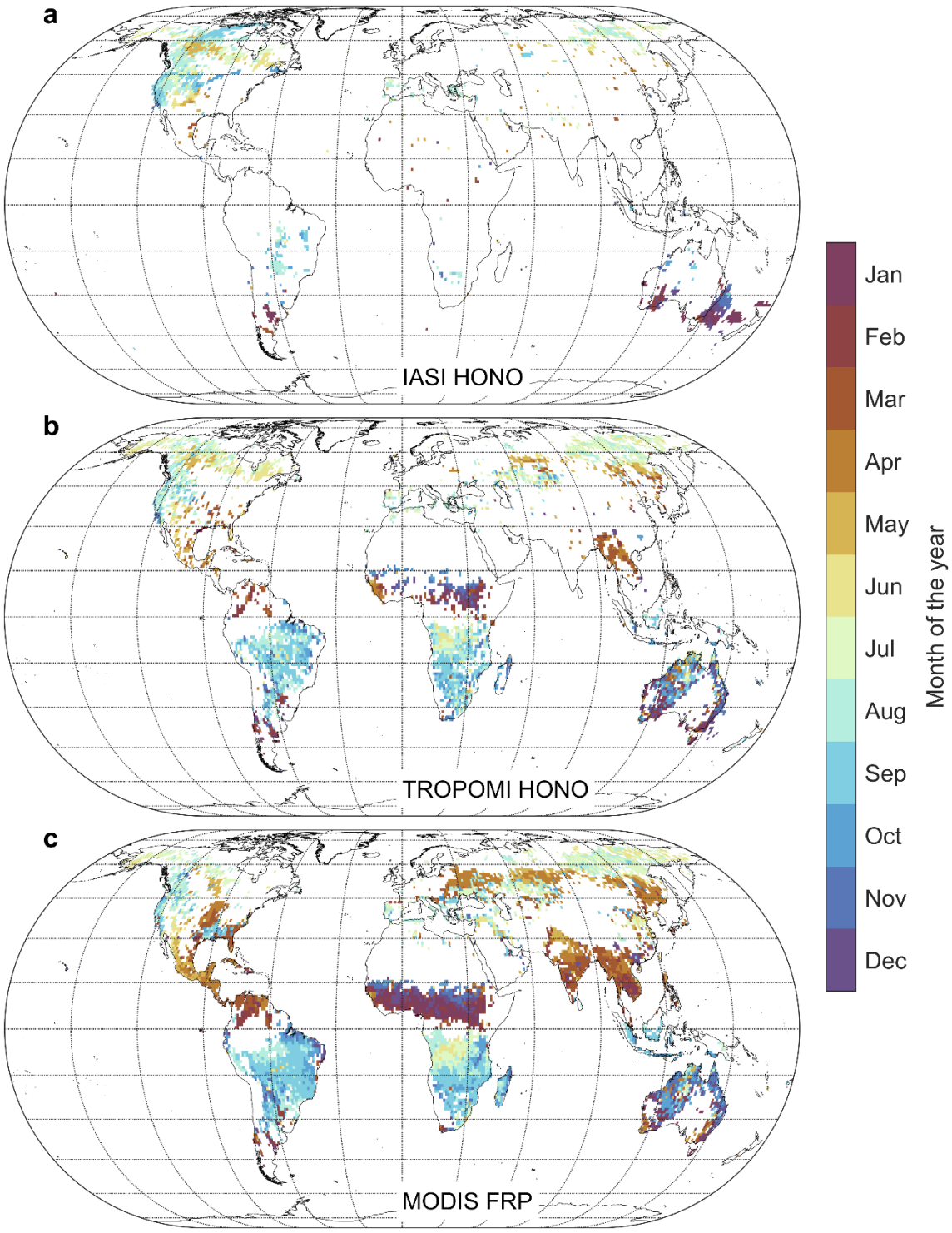

Line 375: the authors should specify what they mean by narrow layer (see main comments).

This is now specified in the manuscript as follows:

"With S_y the generalized covariance matrix of IASI used in the calculation of the HRI (see Sect. 2.1), and K_z the spectral Jacobian with respect to HONO distributed vertically following a Gaussian profile peaking at the altitude z (for z values ranging between 0 and 14 km altitude) and with a standard deviation (σ) of 300 m around z, representing a narrow atmospheric layer."

Line 445 and around when the authors discuss the difference between the early time series and the more recent ones: at the beginning of IASI-A lifetime, only one pixel out of two was distributed. In the time series presented here, is it still the case or all the pixels are considered? If not, this may impact the number of detections for this period.

In the early IASI time series, all Level-1 data were distributed, but Level-2 data (temperature, water vapour, etc.) were indeed only available for one pixel out of two. However, for the IASI HONO product and the other ANNI v4 products (e.g., NH_3 and C_2H_4), we use ECMWF ERA5 reanalysis data (Hersbach et al., 2020) instead of IASI Level-2 data throughout the IASI time series. Moreover, we use our own cloud product, derived directly from IASI radiances (Whitburn et al., 2022). This allows us to exploit consistently all the observations from the IASI time series for both HRI detection and retrieval of HONO.

Line 477-492: It is not clear for me to what conclusion for HONO the analysis of ethylene leads.

We agree with the Referee that we did not motivate enough the analysis of C_2H_4 in Sect. 3.2. This is now done as follows:

"*To rule out potential other reasons for the observed am/pm difference, it is useful to look at another short-lived biomass burning tracer, namely C_2H_4. In Fig. 12, we compare […]*

[…] Although reactions with OH and O_3 are expected to proceed more slowly during nighttime hours due to lower temperatures, we do not observe a prevalence of C_2H_4 detections with the evening IASI measurements, such as observed for HONO (Fig. 12). This suggests, first, that variations in photochemistry between daytime and nighttime do not significantly impact C_2H_4 concentrations in fire plumes. Second, it implies that the presence of measurement artefacts responsible for large am/pm differences in HONO detection can be ruled out, confirming that the absence of photolysis is the primary driver of the more numerous HONO detections at nighttime."

Line 518: What do the authors mean by "actual retrieval"? Is it the retrieval based on a radiative transfer model, or is it the ANNI retrieval?

We meant "*the ANNI retrieval*". This has been corrected.

Section 4.3, discussion of the Woosley Fire: the authors elaborate on the time evolution and the spatial extension of the plumes using IASI and TROPOMI observations. I would be more cautious about what we can draw from these comparisons, given the assumptions and the large uncertainties in the observations and the differences in terms of sensitivity of the two instruments.

We agree with the Referee that the discussions in Sect. 4.3 are not straightforward given the uncertainties and instrumental differences. This is why, in the second paragraph of Sect. 4.3, we alert the reader: "*The goal here is not to perform a quantitative cross-validation of the two satellite products. Comparing at face value the IASI and TROPOMI VCDs of HONO is indeed particularly challenging given the intrinsic differences between the two satellite sounders. The main ones are: […] For these reasons, the primary objective is to showcase the ANNI v4 HONO product and to provide a qualitative assessment of the HONO VCDs from IASI and TROPOMI.*"

In addition, we further discuss the IASI/TROPOMI disparities and their impact on HONO measurements in Sect. 4.4. Notably, we write at the beginning of Sect. 4.4: "*Despite improvements, the retrieval of HONO VCDs in fire plumes from both IASI and TROPOMI remains challenging and currently requires assumptions that introduce uncertainties on the retrieved quantities and hinder a more accurate comparison between their respective HONO products.*"

We reiterate these caveats in the conclusion: "*The HONO columns from these two sounders show promising results with retrieved VCDs in the same order of magnitude. Nonetheless, this comparison cannot serve as cross-validation of the satellite products, given the distinct characteristics and overpass times of the two sounders.*"

Technical corrections:

Figures quality when printed is low.

We thank the Referee for bringing this point to our attention. We created the manuscript's PDF with LaTeX, utilizing figures saved in a vectorized format. Upon examination, the figures appear satisfactory even when zoomed in on screen. We commit to ensuring the use of figures with the highest quality in the next steps.

Figure 3: the colorbars should be reversed. C2H4 colorbars is below NH3 plots and vice versa.

The colorbars in Fig. 3 are correct. The x-axis of the panels in the left column indicates the NH_3 HRI of the observations displayed in the scatter plots, and these observations are colour-coded based on their C_2H_4 HRI (colorbar). The panels in the right column depict the same relationships, but with the C_2H_4 HRI on the x-axis and the NH_3 HRI as the colour code. We have also slightly modified this figure to enhance its clarity.

Line 481: change "The IASI retrieval" to "The IASI detection".

Done. Thank you for spotting this mistake.

References

- Clarisse, L., Hurtmans, D., Prata, A. J., Karagulian, F., Clerbaux, C., De Mazière, M., and Coheur, P.-F.: Retrieving radius, concentration, optical depth, and mass of different types of aerosols from high-resolution infrared nadir spectra, Applied Optics, 49, 3713, https://doi.org/10.1364/ao.49.003713, 2010.
- Clarisse, L., Coheur, P.-F., Prata, F., Hadji-Lazaro, J., Hurtmans, D., and Clerbaux, C.: A unified approach to infrared aerosol remote sensing and type specification, Atmospheric Chemistry and Physics, 13, 2195–2221, https://doi.org/10.5194/acp-13-2195-2013, 2013.
- Clarisse, L., Clerbaux, C., Franco, B., Hadji-Lazaro, J., Whitburn, S., Kopp, A. K., Hurtmans, D., and Coheur, P.-F.: A Decadal Data Set of Global Atmospheric Dust Retrieved From IASI Satellite Measurements, Journal of Geophysical Research: Atmospheres, 124, 1618–1647, https://doi.org/10.1029/2018jd029701, 2019.
- Franco, B., Clarisse, L., Van Damme, M., Hadji-Lazaro, J., Clerbaux, C., and Coheur, P.-F.: Ethylene industrial emitters seen from space, Nature Communications, 13, 6452, https://doi.org/10.1038/s41467-022-34098-8, 2022.
- Hersbach, H., Bell, B., Berrisford, P., Hirahara, S., Horányi, A., Munoz-Sabater, J., Nicolas, J., Peubey, C., Radu, R., Schepers, D., Simmons, A., Soci, C., Abdalla, S., Abellan, X., Balsamo, G., Bechtold, P., Biavati, G., Bidlot, J., Bonavita, M., Chiara, G., Dahlgren, P., Dee, D., Diamantakis, M., Dragani, R., Flemming, J., Forbes, R., Fuentes, M., Geer, A., Haimberger, L., Healy, S., Hogan, R. J., Hólm, E., Janisková, M., Keeley, S., Laloyaux, P., Lopez, P., Lupu, C., Radnoti, G., Rosnay, P., Rozum, I., Vamborg, F., Villaume, S., and Thépaut, J.-N.: The ERA5 global reanalysis, Quarterly

Journal of the Royal Meteorological Society, 146, 1999–2049, https://doi.org/10.1002/qj.3803, 2020.

- Van Damme, M., Clarisse, L., Franco, B., Sutton, M. A., Erisman, J. W., Kruit, R. W., van Zanten, M., Whitburn, S., Hadji-Lazaro, J., Hurtmans, D., Clerbaux, C., and Coheur, P.-F.: Global, regional and national trends of atmospheric ammonia derived from a decadal (2008-2018) satellite record, Environmental Research Letters, 16, 055 017, https://doi.org/10.1088/1748-9326/abd5e0, 2021.
- Whitburn, S., Van Damme, M., Clarisse, L., Bauduin, S., Heald, C. L., Hadji-Lazaro, J., Hurtmans, D., Zondlo, M. A., Clerbaux, C., and Coheur, P.-F.: A flexible and robust neural network IASI-NH3 retrieval algorithm, Journal of Geophysical Research: Atmospheres, 121, 6581–6599, https://doi.org/10.1002/2016jd024828, 2016.
- Whitburn, S., Clarisse, L., Crapeau, M., August, T., Hultberg, T., Coheur, P. F., and Clerbaux, C.: A CO2-independent cloud mask from Infrared Atmospheric Sounding Interferometer (IASI) radiances for climate applications, Atmospheric Measurement Techniques, 15, 6653–6668, https://doi.org/10.5194/amt-15-6653-2022, 2022.

Pyrogenic HONO seen from space: insights from global IASI observations.

https://doi.org/10.5194/egusphere-2023-2707

Response to Referee #2

In their manuscript, "Pyrogenic HONO seen from space: insights from global IASI observations," the authors present a new retrieval of HONO from biomass burning using the infrared sounder IASI. Franco et al. identify two absorption bands (820-890 cm-1 and 1210-1305 cm-1) for optimal use in the calculation of the hyperspectral range index (HRI), used in the detection of HONO. The authors demonstrate that the 1210-1305 cm-1 absorption band has the least interferences with ammonia (NH3) and dust in the Middle East. They reduce false detections of pyrogenic HONO by also using co-located NH3 and C2H4. Instead of focusing solely on individual fires as previous studies have done, the authors also present a global HONO detection climatology of fires from 2007 to 2023, analyzing HONO detection location, aerosol height, MODIS FRP count and mean FRP, and detection time of year. These parameters are compared against the TROPOMI UV-Vis HONO retrieval and a discussion about the differences in retrieval quality between the two instruments is provided. IASI is capable of outputting trace gas retrievals during the daytime and nighttime, and the authors use the number of IASI HONO detections and case studies to form hypotheses about the HONO diel cycle. Finally, Franco et al. use a neural network, ANNI, to compute HONO vertical column densities. These are qualitatively compared to TROPOMI.

This paper demonstrates a new and groundbreaking retrieval of pyrogenic HONO using infrared sensing that allows for long-term analysis of HONO and sub-diurnal observations without the aerosol sensitivity that the UV-Vis retrieval has. HONO has been shown to be critical in the early stages of fire plumes as it is the majority source of OH due to its short photolytic lifetime. How varying sunlight impacts HONO lifetime within smoke is a crucial topic of interest given its oxidative importance. This retrieval is also prime for use on new geostationary satellite (MTG-IRS) which will make observations has frequent as every half hour. This paper is thorough, well-structured, and written well. The limitations of each HONO retrieval method (IASI IR vs TROPOMI UV-Vis) are discussed and reiterated throughout the manuscript and was very appreciated by this reviewer. I recommend this paper for publication subject to minor revisions.

We thank the Referee for the positive evaluation of the paper and for the constructive comments that helped improving the manuscript. Please find in blue here below our answers to the Referee's comments and the changes made to the manuscript. Additionally, we have updated some figures to enhance their clarity. Furthermore, we have revised several figures to improve both their clarity and consistency across the entire manuscript.

General Comments:

I thought the authors did a great job presenting their work, arguments, and conclusions to the reader. The following are a few general comments:

The authors ultimately decided to show many of their results using the 1210-1305 cm-1 window due to the limitations shown for the 820-890 cm-1 window (NH3 interference and Middle East dust interference) and I was curious why this window was included for earlier discussion in the paper. The

conditions defined in lines 252-253 made me wonder why this is defined since it has a demonstrated surface emissivity anomaly and NH3 interference. Line 285 also mentions using the two different HONO HRIs right after the authors state that only the 1210-1305 cm-1 window would be used from then on. It would make for a cleaner story if the 820-890 cm-1 window was not included at all and just summarized as a window that was up for consideration.

We thank the Referee for this comment. Throughout Sect. 2, we systematically examined both the 820-890 and 1210-1305 cm^{-1} spectral ranges for HONO detection. We firmly believe that, especially at this stage of the manuscript, it is crucial to give equal consideration to both bands. Notably, the 820-890 cm^{-1} absorption feature led to the first identification and retrieval of HONO with infrared satellite sounders (Clarisse et al., 2011; Dufour et al., 2022). Therefore, in Sect. 2, we conducted various exercises to evaluate both bands, including a comparison of HRI intensity in fresh fire plumes (Sect. 2.2), a thorough spectral analysis with the whitening (Sect. 2.3), and a comparison of the specific detection filters set up for each absorption band (Sect. 2.4). While we concluded Sect. 2.4 by specifying our focus on the 1210-1305 cm^{-1} HRI for the rest of the study, we deliberately included some results from the 820-890 cm^{-1} range in our analysis in Sect. 3 (and related figures in appendix) as it allows us to perform comparisons between the two HONO bands. The consistency observed in our results across these two ranges provides indeed valuable cross-verification, bolstering the robustness of our findings. We are convinced that this approach is important for establishing the reliability of our methodology and results, and that it enhances the overall strength and credibility of our study.

To clarify our approach, we have added the following statements, respectively, in Sect. 2.1 and at the end of Sect. 2.4:

Line 132: "*Throughout Sect. 2, we systematically assess the advantages and limitations of each spectral range for the detection of pyrogenic HONO.*"

Line 278: "*Considering the advantages presented in Sect. 2 of the 1210-1305 cm^{-1} band for the detection of pyrogenic HONO by IASI, we will focus on the HRI calculated within this range from Sect. 3 onwards. Nonetheless, results obtained with the 820-890 cm^{-1} band will also be presented briefly, as they allow for important cross-verification.*"

Many of the figures referenced in the paper do not have the subpanels added to direct the reader to the specific panel the authors are referring to. For example, line 192 talks about the retrieved spectrum, which is in Figure 2a, line 203 talks about NH3 interferences, which is in Figure 2b, line 258 talks about non simultaneous detection of NH3 and C2H4, which can be easily seen in Figures 3c, d, and h, etc. These cues make it easier for the reader to follow the authors' line of thought.

We thank the Referee for this suggestion, which contributes to enhancing the paper's clarity. In the revised manuscript, we have increased the frequency of references to figures, specifically pinpointing relevant panels crucial to the ongoing discussion.

Specific Comments:

Figure 1: I suggest adding wind vectors over each panel to demonstrate where the HONO is being transported from. I think it would be especially helpful in Figures 1c and 1d, the October 15, 2017 9:30 PM overpass. Additionally, it would aid the reader if a general HRI = 4 contour was included in each subfigure. Finally, I suggest making the red cross either a square or a thick outline. My initial thought was that a red cross meant bad data, ignore this.

We thank the Referee for these suggestions. Please find below the revised version of Fig. 1.

- Panels c and d incorporate the wind vectors associated with each IASI/Metop-A observation, derived from the daily horizontal wind fields from the ECMWF ERA5 reanalysis (Hersbach et al., 2020). The wind is oriented to the North and carries the fire plume above the Bay of Biscay.
- Unfortunately, adding an HRI = 4 contour line was not feasible due to significant variations in HONO HRI among nearby IASI observations and the discontinued spatial sampling. However, to enhance differentiation between HRI>4 and HRI<4 observations, we have modified the colour palette, which is now discretized, and IASI observations with HRI<4 are displayed with semi-transparency.
- We have replaced the red cross by a light blue square around the observation of interest.

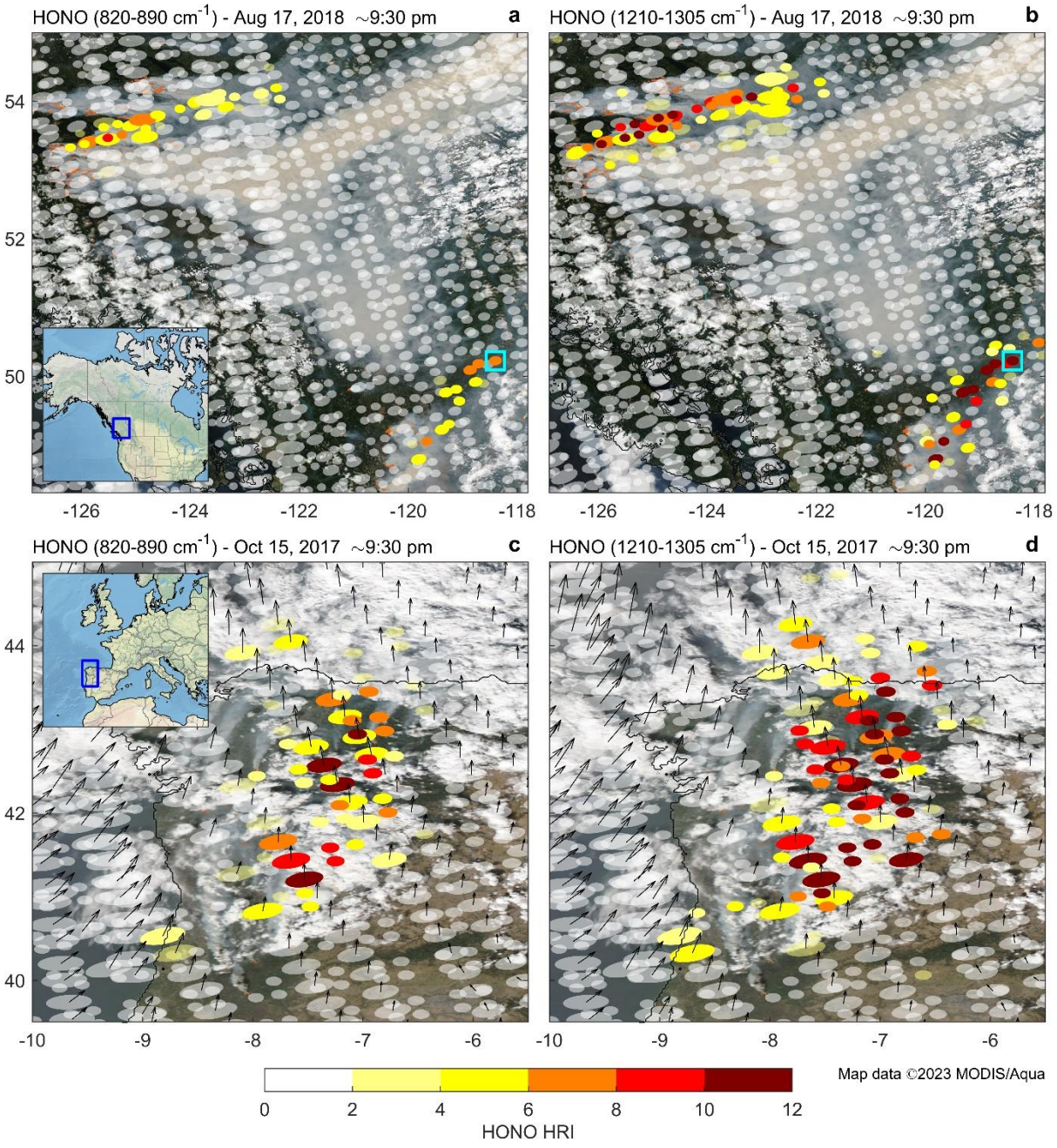

Line 195: Could the authors include an appendix figure covering the entire spectral interval? It makes me curious why 1210-1250 cm-1 was omitted.

The figure below displays Fig. 2, including the entire 1210-1305 cm^{-1} spectral range in panel c and the whitened NH_3 Jacobian. The 1210-1250 cm^{-1} range shows no significant contribution of HONO to the HRI, and there is no interference from NH_3, as NH_3 lacks absorption features in that part of the spectrum. We intentionally selected a wide range (1210-1305 cm^{-1}) for calculating the HONO HRI to provide more baseline, reducing issues related to, for example, surface emissivity. However, for better visibility of the HONO absorption features around 1264 cm^{-1}, we prefer to zoom in on the 1250-1305 cm^{-1} range in Fig. 2.

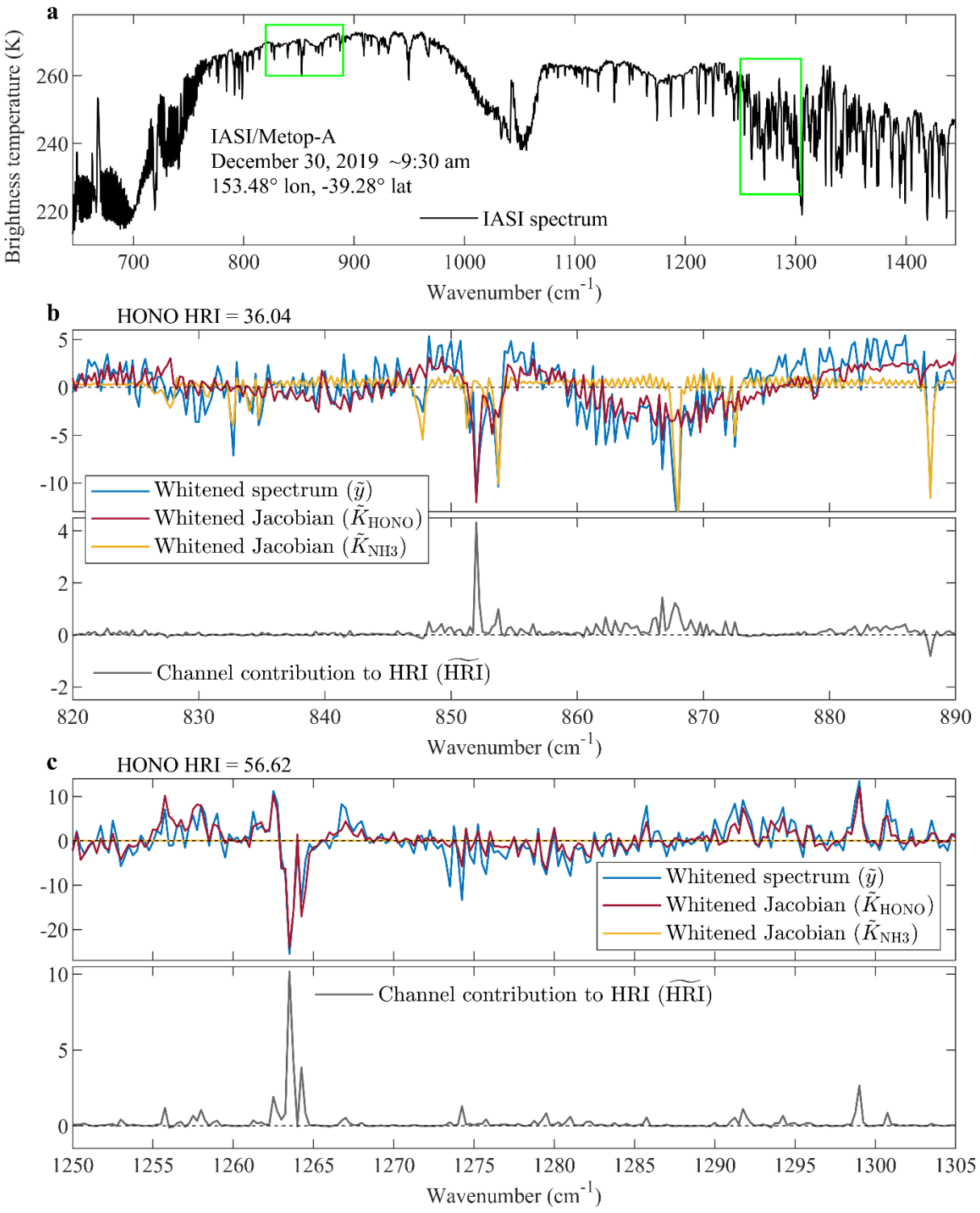

Section 2.3: I was confused what the author meant by the term "channel," as in the channel contribution to HRI. I first thought it was for each individual compound, but then Figure 2b talks about the channel contribution to HRI for both HONO and NH3 referencing the same line. It may have been defined in a referenced paper or it may be common terminology in this specific field. However, I would like more context or a clear definition.

A “channel” is defined here as the observed IASI radiance at a specific wavenumber. It corresponds to a single spectral band sampled at 0.25 cm^{-1}, which is the spectral resolution of IASI (after apodization). We have added this definition to the manuscript.

Figure 2: Could the whitened Jacobian for NH3 also be added to c? Would this further demonstrate a lack of interference from NH3?

We appreciate the suggestion from the Referee. We have now included the whitened NH_3 Jacobian in panel c of Fig. 2 (and in the other similar figures in the appendix). As mentioned earlier, NH_3 lacks absorption features in that part of the spectrum and, therefore, cannot influence the HONO HRI in that band.

Line 232: Can these localized surface emissivity anomalies be accounted for in the retrieval or are they time-varying properties?

A first-order correction could be applied by estimating the spatially variable biases from a period in the year (usually the winter), as done by Clarisse et al. (2019) for the retrieval of dust from IASI. The prerequisite of such approach is to assume that the emissivity and corresponding bias is constant throughout the year (or at the least has less variability than the bias itself). However, the surface emissivity anomalies affecting the 820-890 cm^{-1} HONO absorptions are spatially too heterogeneous, too intense, and too time-of-the-year-dependent to be efficiently accounted for.

Figure 3: Is there any reason why it looks like there are more than two populations in the HONO vs NH3 colored by C2H4 figures (Figures 3a, c, e, and g)? It is especially apparent in 3a, where a linear trend of yellow dots seems distinct from the pink/orange dots of higher NH3, but lower HONO. Could the authors discuss this? It may be relevant to the biomass type and region comment in lines 257-258.

The population highlighted by the Referee in Fig. 3a (for the 820-890 cm^{-1} range), also noticeable in Fig. 3e (for the 1210-1305 cm^{-1} range), is mainly associated with the 2009 and 2019/2020 Australian wildfires. This population is less evident in the scatter plots including the pm observations (Figs 3c and g), given that the number of HONO detections is roughly 10 times higher in nighttime than in daytime. What is notable about these specific events is that they resulted in numerous HONO detections during both daytime and nighttime overpasses, with particularly high C_2H_4 HRI values but not very high NH_3 HRI values compared to other fire events. Various factors, such as the type of vegetation burned, high loads of smoke aerosols (which are hypothesized to shield the HONO burden from efficient photolysis, extending its lifetime), and intense pyroconvection transporting fire plumes to the lower stratosphere where photochemistry is slowed drastically (increasing competition for OH), are among many elements that can explain the specificity of Australian fire plumes. Although we agree with the Referee that delving further into the population of points in Fig. 3 is undoubtedly interesting, we believe it is not possible to do so within the framework of this paper and that it would deserve a dedicated study.

Line 289-290: Is there any other data that would explain these random detections over remote ocean?

The HONO detection filter we set up effectively mitigates random detections over remote oceans. Nevertheless, given the extensive IASI time series, it is conceivable that a limited number of observations might bypass the filter, though such instances remain largely marginal, as evident in Figs 4 and A5. These random detections constitute only ~20 instances out of the >10 x 10^9 observations in the entire IASI time series. We identify ice clouds, characterized by broadband infrared observations, as a potential interference leading to these random detections. For instance, in Fig. 4, two of these random detections are visible over Antarctica.

Line 316: The authors later go into an analysis of why there are detections lacking in the global tropics (sect 3.2), but I was curious what is the effect of clouds on the retrievals? I know that the authors included cloud and cloud-free spectra, but there wasn't a comment on how clouds affect the retrieval. I asked myself if the ITCZ had any effect? This may be showing my lack of IR expertise.

The HRI has indeed been built based on a subset including cloudy and cloud-free spectra, ensuring that the HRI remains unbiased for all atmospheric conditions. However, if the cloud coverage is too thick and extensive, the detection of HONO will be impeded (the HRI values will be very weak), and the IASI measurements will simply not pass the HONO detection filter, and no retrieval will be performed. This implies that the retrieval of HONO is primarily conducted for cloud-free scenes and for observations with a limited cloud cover. Such residual clouds typically impact the baseline of the spectra. However, since we use surface temperature instead of a baseline temperature derived from the spectrum, the residual clouds have only a marginal impact on the HONO detection and retrieval. Additionally, in the final product, we provide a cloud flag that allows the user to discriminate between clear-sky, partially cloudy, and cloudy scenes.

We do not believe that the ITCZ plays a role in the small number of HONO detection within the Tropics. For instance, during the Northern Hemisphere winter (Nov – Feb), the ITCZ moves southward, leading to dry and hot weather in western and central Africa. This corresponds to the biomass burning season, as shown in Fig. 5. Even though the ITCZ is located to the south during this period, IASI does not detect HONO during the fire season of these regions.

Figure 5: I found it interesting that IASI HONO saw detections off the coast of Australia, over water. How does this retrieval do over water? There was a large discussion of the thermal contrast affecting the retrieval. Were these plumes detected because they were over water or because the strength of the fires had lofted them high enough for key detection?

The ANNI v4 retrieval performs equally well over both land and sea. The crucial factor lies in the ability to detect HONO, which is largely dependent on thermal contrast. Typically, thermal contrast is weaker over water than over land. However, the Australian wildfires are well known for their intense pyroconvection that swiftly lifted concentrated PyroCb to the UTLS, reaching altitudes of 14-16 km off the coast of Australia. The air temperature at such altitudes is very low, resulting in a very large thermal contrast with the surface. Both the large thermal contrast and the high concentrations in trace gases favoured the detection of HONO over water during these fire events.

Equation 6: I'm not sure why this equation is presented, if only to demonstrate height dependence on the detection threshold. When the authors talk about the NN VCD calculation in section 4, I was wondering if this equation was used or not.

Eq. 6 is used in Sect. 3.2 to characterize the HONO VCD that corresponds to the IASI generalized noise, and hence to the detection threshold, for a standard atmosphere, depending on the plume altitude. However, as explained in Sect. 4.1, the actual retrieval of the HONO VCD for a single IASI observation is performed using an artificial NN. This NN is provided with the single pixel HRI – and ancillary variables describing the state of the surface and atmosphere – and yields an estimate of the HONO VCD. Eq. 6 does not play a role in this process.

Line 376: This line made me wonder what the height limitations are on HONO detection with IASI.

The detection of HONO with IASI is particularly challenging in the lowermost atmospheric layers, especially in the planetary boundary layer, owing to the overall weak thermal contrast between the surface and these layers. As illustrated in Fig. 7, detecting HONO in these low layers with IASI

necessitates a substantial abundance of HONO, typically exceeding 2.5-3 x 10^{16} molec cm^{-2}, a condition that is rarely met.

Line 377: The authors spend a lot of time explaining their constraints for IASI HONO detection, but not a lot of time is spent explaining the constraints on valid TROPOMI HONO detections, which are frequently compared against.

While the scope of this study is HONO measurements with IASI, the manuscript also addresses constraints affecting HONO detections and retrieval with TROPOMI. For instance:

- The presence of smoke aerosols hindering TROPOMI from probing through the full height of the smoke plume is discussed in Sect 4.4.
- The difficulty in estimating the AMF to convert TROPOMI's SCDs to VCDs is also discussed in Sect. 4.4. Moreover, for a comprehensive description of TROPOMI's detection and retrieval, including limitations, readers are referred to Theys et al. (2020).
- As noted in the introduction, UV-Vis instruments like TROPOMI do not provide measurements during nighttime, when HONO's lifetime is expected to be the longest. Moreover, the manuscript discusses the impact of TROPOMI's overpass time (~1:30 pm), which coincides with the time of the day when HONO photolysis is most efficient.
- In Sect. 3.2, there is a discussion about the typical TROPOMI's detection threshold for HONO, which is significantly lower than IASI, and relatively homogeneous throughout the troposphere since, unlike IASI, TROPOMI's measurements are not influenced by the thermal contrast.

Line 390: Why is volcanic ash included?

While we do not anticipate any HONO detections associated with volcanic plumes, we have observed several instances in the CALIPSO data where "elevated smoke" was mistakenly classified as "volcanic ash", and vice versa.

Line 395: Did your analysis lead to the conclusion that layers between 2 and 4 km contained many false detections? I'd like to see this in an appendix figure or have a paper cited.

We realize that our statement in Lines 396-397 was misleading. What we meant to convey is that the low-altitude layers between 2 and 4 km can be influenced by anthropogenic pollution plumes exiting the planetary boundary layer, while in this study, we primarily measure HONO in mid- and high-altitude plumes. We have corrected our sentence: "*[…] numerous low-altitude layers comprised typically between 2 and 4 km, which may be influenced by anthropogenic pollution plumes.*"

Figure 8: Please add latitude labels.

We tried adding labels but found these too distracting. We clarified them instead in the caption: "*Parallels are drawn every 15° and meridians every 30°.*" For consistency, we did the same for the other figures using the same type of projection in the manuscript (Figs 5, 6, 8, and 12).

Figure 9: Are the MODIS fire detections in comparison to TROPOMI from Aqua or Terra, or both? Should TROPOMI be compared to the closest overpass? Or what about in comparison to VIIRS which has a very close overpass time to TROPOMI?

We thank the Referee for this question. So far, we have compared both IASI and TROPOMI to MODIS/Terra in Fig. 9. We agree that it is indeed more appropriate to compare TROPOMI with MODIS/Aqua, which has a coincident overpass time with TROPOMI (~1:30 pm). Please find the revised version of Fig. 9 below. Considering the similarities between the MODIS/Terra and MODIS/Aqua

distributions, note that the entire discussion and the conclusions related to this figure in the manuscript remain entirely valid.

Since MODIS/Aqua has a coincident overpass time with TROPOMI, we prefer to work only with MODIS for consistency throughout the manuscript and to avoid introducing an additional satellite dataset in the study.

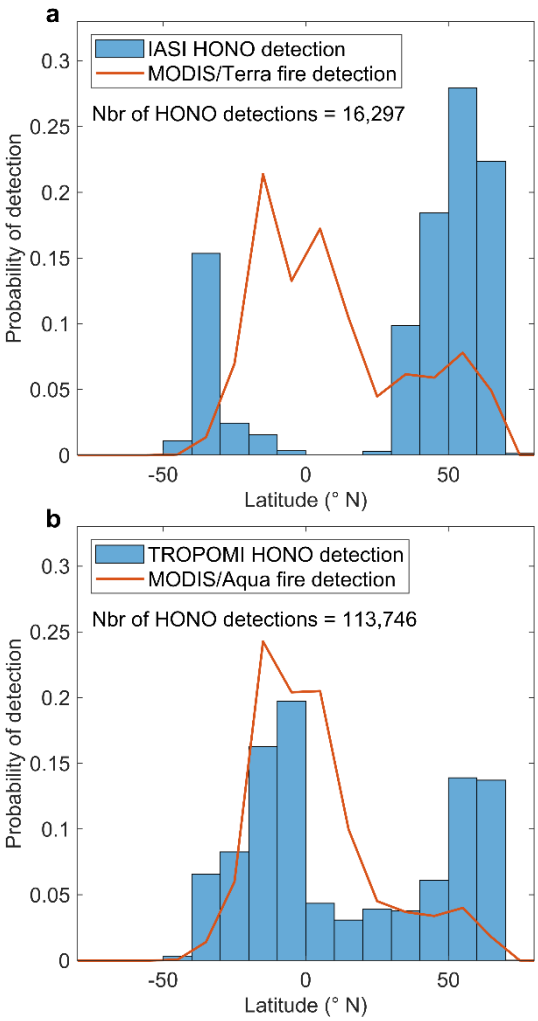

Figure 10: I may have missed it, but is there a reference comparing the differences between IASI-A, -B, and -C? I am seeing slight differences between the three instruments, though the authors show similar annual counts of HONO detections in Figure 11.

Overall, the three IASI instruments demonstrate excellent agreement during their overlapping years (Bouillon et al., 2020). The slight differences seen between IASI-A, -B, and -C in Fig. 10 are due to small variations in overpass times (~30 min) and spatial shifts between the tracks of the three Metop satellites. For instance, despite the 2200 km swath covered by a single IASI instrument, gaps exist in the Tropics between the successive orbits of this instrument. The tracks of the other instruments are set up to cover the tropical gaps left by the first instrument. Consequently, a specific fire plume is never sampled simultaneously, and with the same spatial coverage, by each IASI instrument, leading to different numbers of HONO detections for these instruments in the same fire plume.

When aggregated over all the fire events detected throughout the course of one year of observation, these differences largely cancel out, contributing to the consistency observed between the three IASI instruments in Fig. 11.

Line 440: What is a confirmed HONO detection?

We consider HONO detections as “confirmed” those that passed the specific filter set up in Sect. 2.4. To avoid creating ambiguities, we have changed "*the number of confirmed HONO detections*" to "*the number of HONO detections*" in this sentence.

Line 452: Has anyone else cited this drop in the year 2022? Not for HONO detections but perhaps in sum FRP? Very interesting.

While we are not aware of recent studies reporting a drop in 2022, considering the devastating biomass burning season in North America in 2023, more studies on the topic will likely emerge. Nonetheless, the Referee’s question has motivated us to investigate this point further. In the revised version of Fig. 11 (below), we have presented the annual cumulative Fire Radiative Power (FRP) from MODIS/Terra for the Northern Hemisphere mid and high latitudes (>30° N) from 2007 to 2022 (the consolidated MODIS dataset is not available yet for the entire 2023). This cumulative FRP is the sum of all individual fire contributions throughout each year, providing a better indicator of integrated biomass combustion than, for example, fire count (which disregards fire magnitude) or average FRP (which ignores the number of fires). For consistency, we now consider only the HONO detections above 30° N since those represent by far most of the detections. In this figure, we observe that the cumulative FRP closely follows the time series of HONO detections, with drops in 2016 and 2022 and a peak in 2021, aligning with the IASI data. This represents additional evidence indicating that HONO detection with IASI depends strongly on fire intensity. We have included this revised figure in the manuscript, and we now discuss this in Sect. 3.3.

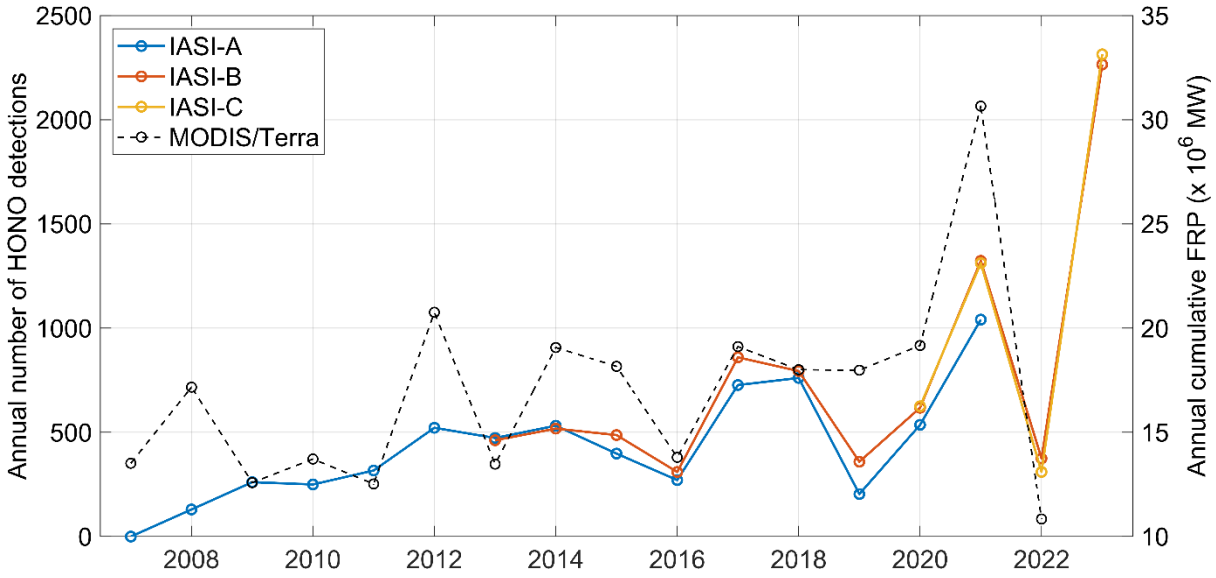

Section 3.4: One paragraph starts by saying “To rule out potential other reasons for the observed am/pm difference…” but then the section doesn’t have an overall concluding statement about HONO’s diel cycle, just about the effect of photochemistry on C2H4

We thank the referee for highlighting this point. We have included the following concluding statement in the C_2H_4 analysis:

“To rule out potential other reasons for the observed am/pm difference, it is useful to look at another short-lived biomass burning tracer, namely C_2H_4. In Fig. 12, we compare […]

[…] Although reactions with OH and O_3 are expected to proceed more slowly during nighttime hours due to lower temperatures, we do not observe a prevalence of C_2H_4 detections with the evening IASI measurements, such as observed for HONO (Fig. 12). This suggests, first, that variations in photochemistry between daytime and nighttime do not significantly impact C_2H_4 concentrations in fire plumes. Second, it implies that the presence of measurement artefacts responsible for large am/pm differences in HONO detection can be ruled out, confirming that the absence of photolysis is the primary driver of the more numerous HONO detections at nighttime."

Technical Corrections:

Line 377: "An HONO detection" to "A HONO detection."

Corrected

References

- Clarisse, L., R'Honi, Y., Coheur, P.-F., Hurtmans, D., and Clerbaux, C.: Thermal infrared nadir observations of 24 atmospheric gases, Geophysical Research Letters, 38, L10802, https://doi.org/10.1029/2011gl047271, 2011.
- Dufour, G., Eremenko, M., Siour, G., Sellitto, P., Cuesta, J., Perrin, A., and Beekmann, M.: 24 h Evolution of an Exceptional HONO Plume Emitted by the Record-Breaking 2019/2020 Australian Wildfire Tracked from Space, Atmosphere, 13, 1485, https://doi.org/10.3390/atmos13091485, 2022.
- Hersbach, H., Bell, B., Berrisford, P., Hirahara, S., Horányi, A., Munoz-Sabater, J., Nicolas, J., Peubey, C., Radu, R., Schepers, D., Simmons, A., Soci, C., Abdalla, S., Abellan, X., Balsamo, G., Bechtold, P., Biavati, G., Bidlot, J., Bonavita, M., Chiara, G., Dahlgren, P., Dee, D., Diamantakis, M., Dragani, R., Flemming, J., Forbes, R., Fuentes, M., Geer, A., Haimberger, L., Healy, S., Hogan, R. J., Hólm, E., Janisková, M., Keeley, S., Laloyaux, P., Lopez, P., Lupu, C., Radnoti, G., Rosnay, P., Rozum, I., Vamborg, F., Villaume, S., and Thépaut, J.-N.: The ERA5 global reanalysis, Quarterly Journal of the Royal Meteorological Society, 146, 1999–2049, https://doi.org/10.1002/qj.3803, 2020.
- Walker, J. C., Dudhia, A., and Carboni, E.: An effective method for the detection of trace species demonstrated using the MetOp Infrared Atmospheric Sounding Interferometer, Atmospheric Measurement Techniques, 4, 1567–1580, https://doi.org/10.5194/amt-4-1567-2011, 2011.